Article

Nanoconfinement of Ionic Liquid into Porous Carbon Electrodes

Francesca Borghi,* Claudio Piazzoni, Matteo Ghidelli, Paolo Milani, and Alessandro Podestà*

Read Online

ACCESS | 📊 Metrics & More | 📖 Article Recommendations | 🆂🅸 Supporting Information

ABSTRACT: Planar electrochemical double-layer capacitors (supercapacitors) are strategic elements for the realization of miniaturized autonomous devices requiring energy storage and conversion capabilities. In particular, supercapacitors fabricated with nanoporous carbon electrodes and ionic liquids as electrolytes are very promising for a wide range of applications. The understanding and control of the interactions of the ionic liquid with the porous carbon interface is both practically and fundamentally interesting, because of the effects of surface confinement on the structural and functional properties of the ionic liquid. In particular, the role of the morphology in the ionic liquid confinement has attracted huge interest in many disciplines. Here we report direct experimental evidence of the solid-like structuring of confined 1-butyl-3-methylimidazolium bis(trifluoromethylsulfonyl) imide ([Bmim][NTf2]), which extends several tens of nanometers from the interface of nanoporous carbon thin films. These solid-like structures coexist with a huge amount of ionic liquid in its bulk phase. The presence of a solid-like phase occurring at the interface affects the double-layer organization of the ionic liquid at the electrified interface of nanoporous carbon based planar supercapacitors. Our results suggest the presence of the solid-like structured ionic liquid domains not only on the upper carbon thin film interface but also into the bulk of the nanoporous matrix.
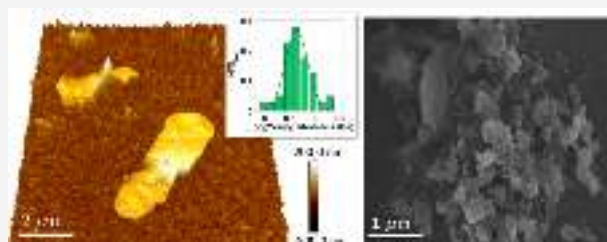
INTRODUCTION

The rapidly increasing demand for portable and wearable ecofriendly energy sources requires the integration of efficient electrical energy conversion and storage devices into flexible and stretchable systems.[1−3] Electrochemical double-layer capacitors (EDLCs)[4,5] are promising candidates for the production of autonomous devices integrated on soft and flexible substrates.[6−8] Among different approaches proposed for the fabrication of planar EDLCs, those based on the use of porous carbon as electrode material,[9,10,4] due to its high surface area and good electrical conductivity,[11,12] and ionic liquids (ILs)[13,14] as electrolytes have demonstrated superior performances.[15] In particular, ILs are more efficient than conventional water-based electrolytes,[16,17] due to their wide electrochemical window and high ion density, good thermal stability, and nonvolatility. Their combination with porous carbon films offers also a good packaging solution.[18]

The confinement of ILs in constrained geometries, where at least one dimension is reduced down to lengths comparable to the ion size, confers to the IL different properties with respect to the bulk phase.[19] The confinement of ILs can be found not only in three-dimensional porous matrices but also in more open geometries where the constraining walls are present only along one or two directions. In general, confinement takes place whenever the interaction of the IL with the constraining surfaces becomes relevant with respect to the mutual interaction of IL ions.[19]

The behavior of ILs confined into porous carbons is receiving great attention by a broad community interested in fundamental and technological aspects.[18−21] The interaction of ILs with highly oriented pyrolytic graphite (HOPG), carbon nanotubes,[22,23] and amorphous or graphitic nanoporous carbon[24,25] has been reported. Enhanced diffusivity of the confined ionic liquids compared to that of the bulk-phase was characterized for carbon nanotubes[26] by means of molecular dynamic simulations and for mesoporous carbon matrix by quasielastic neutron scattering experiments.[27,28]

The behavior of the first layers of confined ionic liquids could be crucial for describing not only the mobility properties of ILs but also their structural ones. Molecular dynamic simulations[10] performed on microporous carbon electrodes showed that the first adsorbed ionic layer inside micropores is formed by one ionic species only, whose total charge balances exactly that of the electrode and is not compensated by the second ionic layer, according to the overscreening effect or Coulombic ordering.[29−32]

The interface roughness and the interconnected porosity, which characterize many materials used for electrochemical

Table 1. Structural Properties of the Carbon Cluster Assembled Thin Films

sample name	substrate coverage	substrate	thickness (nm)	roughness (nm)	porosity (%)	specific surface area (m^2/g)
SMP1	sub-monolayer	oxidized silicon	55 ± 9	13 ± 1.7		
SMP2	full coverage	oxidized silicon	150 ± 15	18 ± 2.3	87	1820

devices and sensors, may also deeply affect the behavior of the confined ionic liquids. In spite of a few studies suggesting complex behavior of confined ionic liquids,[33−35] the role of interfacial geometry is currently poorly understood. Furthermore, the reported results concerning the peculiar effects of the confinement of ionic liquid into porous carbon matrix are still controversial; for example, Rajput et al.[35] reported how the presence of an interconnected network of heterogeneous carbon pores reduces the effects due to confinement, causing the ionic liquid to behave similarly to the bulk phase.

Among different types of nanostructured carbons, cluster-assembled nanostructured carbon films (ns-C) produced by supersonic cluster beam deposition (SCBD)[36] are characterized by high porosity (average porosity of ∼78%)[37] and specific surface area ($A_{BET} \approx 1500$ m^2/g);[37] recently we demonstrated the combination of ns-C films produced with imidazolium-based ILs for the production of planar EDLCs,[6,38] easily integrated onto flexible substrate.[39,40]

Here we report the effects of the confinement of ionic liquids into nanostructured porous carbon produced by SCBD. The IL confinement in these nanoporous carbon thin films is realized inside the porous matrix, characterized by pores at the nanoscale,[37] and on the upper surface, characterized by overhangs and a rough interface, which can isolate ionic liquid domains and form discontinuous ionic liquid thin films.

Local solid-like structures[19,41] of 1-butyl-3-methylimidazolium bis(trifluoromethylsulfonyl) imide ([Bmim][NTf2]) confined at the interface with ns-C films[42,43] form and persist in their solid state even when the carbon surface is completely wetted by the ionic liquid, which extends several micrometers from the interface in its bulk phase. According to the phenomenon of formation of solid-like ionic liquid domains previously observed on rough oxidized silicon substrate[41] and on flat oxidized silicon, mica, and glass,[44,45] the term "solid-like" not only refers to an interfacial ordering of the ionic liquid, as is observed for the solvation layers of liquids at solid surfaces,[46,47] but also concerns a transition, which implies the change of many of its structural and functional properties.[45,48]

The macroscopic response of a planar ns-C based supercapacitor with a predeposited thin film of ionic liquid confined into the carbon matrix has been investigated; a particular effort has been made to correlate the description of the ionic liquid behaviors at the nano- and mesoscale to the overall behavior of the device.

■ MATERIALS AND METHODS

Deposition of Cluster-Assembled Carbon Thin Films. Nanostructured porous carbon films have been produced with a SCBD[49] apparatus, equipped with a pulsed microplasma cluster source (PMCS)[50] to deposit ns-C thin films assembled by clusters produced in the gas phase. The PMCS operation principle is based on the ablation of a graphite target rod (6 mm in diameter) by an inert gas plasma jet (helium in this case), ignited by a pulsed electric discharge. The ablated species thermalize with helium and condense to form clusters characterized by a diameter ranging from 0.7 to 2 nm,[37] organized prevalently in amorphous sp^2 carbon and few

disordered graphitic sheets randomly distributed[43] and characterized by an irregular curved surface.[51] The mixture of carbon clusters and helium is then extracted into the vacuum through a nozzle to form a seeded supersonic beam, which is collected on a set of oxidized p-doped silicon (110) wafer fragments (1 cm × 2 cm) intercepting the beam in a deposition chamber. The primeval incident carbon clusters stick on the ones predeposited on the silicon substrate and form a porous nanostructured thin film, whose mean density[37] is 0.42 ± 0.08 g/cm^3. The surface defects and the chemical compounds adsorbed on the surface are homogeneously distributed on the carbon surface, as investigated by Raman spectroscopy and X-ray photoelectron spectroscopy (XPS) measurements published in refs 43 and 52. Samples of carbon cluster-assembled thin films with two different thicknesses (as reported later on in Table 1) have been deposited in order to study with AFM the interfacial properties of confined [Bmim][NTf2] on them.

Planar nanostructured supercapacitors have been fabricated, according to the scheme explained in ref 38, by depositing a nanostructured carbon thin film (150 nm thick) by SCBD on a glass substrate, previously coated with two 200 nm thick evaporated gold film electrodes used as electron collectors, covering an area of 1.2 cm^2 and separated by a 0.6 mm gap. The stencil masks, used during the evaporation of the gold before and the nanostructured carbon depositions later on, have been realized by a Zeus 3DL printer (3DLine) in poly(lactic acid) (PLA). In the Supporting Information, the stencil masks and the planar supercapacitors are shown in Figure S1.

Deposition of [Bmim][NTf2]. We deposited [Bmim]-[NTf2]/methanol (1:1000) diluted solution by drop-casting method, in order to deposit a few nanoliters of ionic liquid on the substrate.

[Bmim][NTf2] (Iolitec, purity ∼99%), whose molecular composition is drawn in Figure 1a, was kept in an ultrahigh vacuum chamber (10^{-6} mbar) for several days before the experiments, in order to reduce water contamination. Methanol (purity 99.8%, HPLC, from Fluka) was distilled twice, in order to decrease the amount of nonvolatile contaminants, as well as the water content. Control measurements have been done by depositing drops of distilled methanol on clean silicon substrates in order to evaluate the complete evaporation of the solvent and the absence of contaminants left on the substrate and hence the efficacy of the solvent cleaning procedure. In fact, we want to exclude any possible contribution from the solvent to the objects formed after [Bmim][NTf2]/methanol solution deposition on the substrate.

The drop-cast deposition was performed in a nitrogen glovebox in order to reduce the presence of water (the residual water content is maintained around 1 ppm during the entire usage time of the glovebox). The effects due to the presence or absence of water in the ionic liquids are widely discussed in literature, as is its controversial influence on the formation of structured ionic liquids;[53−56] for this reason we decided to
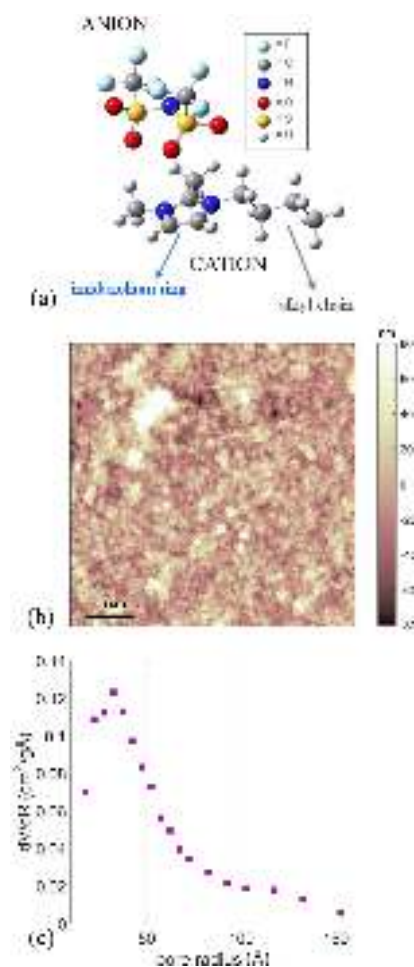
Figure 1. (a) Molecular drawing of [Bmim][NTf2]; (b) top-view AFM morphological map of SMP2; (c) pore radius distribution of SMP2 characterized by nitrogen adsorption technique.

control its presence in the process of structured ionic liquid formation.

A 10 μL droplet of diluted (1:1000) [Bmim][NTf2]/methanol solution was deposited onto the ns-C thin films, and the solvent was left to evaporate completely overnight before the deposited sample was exposed to ambient air for the duration of the AFM characterization.

Structural and Porosity Characterization. The morphological investigation of the carbon nanostructures and of the ionic liquids at the interface was performed with a Multimode 8 AFM (Bruker), in different modes depending on whether the measurements were carried out in air or in liquid environment. Morphologies in air were acquired in tapping mode, while force versus distance/indentation curves were done according to a point and shoot strategy (as explained in the next section); NCHV probes from Bruker, with resonance frequency around 300 kHz, force constant $k = 40$ N/m, and nominal tip radius 8 nm, were used for these experiments. From flattened AFM images, several morphological properties were evaluated. In particular, the root-mean-square surface roughness, R_q, was calculated as the standard deviation of surface heights.[57] The interface between ns-C thin films and the ionic liquid, covered by several hundreds of nanometers of ionic liquid in bulk phase, was characterized in peak-force

tapping mode, with silicon nitride cantilevers mounted with single crystal silicon tips, with nominal radius 12−30 nm, resonance frequency in the range 100−200 kHz, and force constant $k = 0.7$ N/m. All the topographic maps have been collected with a sampling resolution of 1−5 nm/pixel using a scan rate of approximately 1 Hz.

SEM images were acquired using a scanning electron microscope (SEM, Zeiss Supra 40). We collected several grayscale images acquired with a 7 kV electron beam at different magnifications (2000−100000 times) with a resolution of 0.5−2 nm/pixels.

Nitrogen gas adsorption measurements were performed to evaluate the specific surface area and the porosity of carbon cluster-assembled thin films, according to the new methodology described in ref 37, which allow the porosity measurements directly on the thin film without reducing it into powder, destroying part of its structure. In particular, gas adsorption measurements were performed employing a Gemini surface area analyzer (Micromeritics, model 2365). Before each measurement, samples were degassed under a constant helium flux at 200 °C for 3 h using a dedicated unit, in order to remove any contaminants that may have been adsorbed on the silicon surface or onto the pores of the nanostructured materials.

Investigation of the Mechanical and Electrochemical Properties of [Bmim][NTf2] Thin Films. Force spectroscopy[58] is a powerful tool used for the evaluation of the local physicochemical surface properties of a sample, even more effective if the technique can be combined with an imaging of the surface studied. This is a surface investigation that can be accurately performed by AFM, and in particular, we chose a point and shoot strategy,[41] which allows us to perform force curves along a grid spanning a precise surface region, located in a topographic map previously acquired by imaging. In particular, through the acquisition of force versus distance curves (force curves, fcs), acquired along 600 nm of ramp size (which is the maximum distance the AFM tip explores toward and away from the carbon cluster-assembled surface in the z-direction during the acquisition of force curves) at 1 Hz, we have investigated the mechanical properties of the nanostructured carbon thin films and the [Bmim][NTf2] structures. The nanomechanical analysis was then performed by fitting the Hertz model[59] to the force curves in the indentation (δ) region, which is small compared to both the probe radius and the IL surface domains, in order to provide the elastic response of the structured IL islands. The measured Young's modulus must be considered as an apparent modulus, since the effect of the finite thickness of the sample was ignored.[60]

Concerning the electrochemical measurements, once the carbon-based planar supercapacitor was produced, a 300 μL droplet of [Bmim][NTf2] was deposited to fill the gap between the two electrodes and impregnate them. The stencil masks were created according to a geometry that minimizes the error associated with the estimation of the area occupied by the ionic liquid. In fact, since the ionic liquid prefers remaining confined into the carbon matrix instead of overflowing on the glass substrate, a bottleneck was created at the end of both the nanostructured carbon electrodes, and part of the gold collector electrodes was left uncovered for electrical contacts (see Supporting Information for more details). Impedance spectra were acquired with a potentiostat/galvanostat (Gamry Ref 600), in the frequency range from 10^{-2} to 10^5 Hz, with a 5 mV AC perturbation amplitude. The

configuration of the electrochemical measurements is shown in Figure S1d in the Supporting Information.

■ RESULTS AND DISCUSSION

Structural Properties of Cluster-Assembled Carbon. The porous and disordered matrix typical of cluster-assembled carbon thin films is characterized by a high mean specific surface area ($A_{spec} \approx 1550 \pm 200$ m^2/g) and a relevant mean porosity ($p \approx 80\%$), depending on the thickness of the film.[37] Figure 1b clearly shows the rough interface of cluster-assembled materials obtained by supersonic cluster beam deposition,[36] and the remarkable gain in specific area due to the use of small nanometer-sized building blocks.[37] In Table 1, the specific porosity and the specific surface area of the carbon thin films investigated in this work are reported. Carbon clusters deposited with helium as carrier gas are characterized by a multimodal diameter distribution, whose main peaks are 0.7, 1.2, and 2 nm.[37] Clusters, characterized by curved irregular geometry,[51] organize at the nano- and mesoscale on the substrate, providing morphological properties to the thin film that evolve with the quantity of mass deposited (which is proportional to the film thickness), according to a simple scaling law.[61,62] In particular, surface roughness, R_q, evolves with film thickness h according to $R_q \approx h^\beta$,[57] where β is the growth exponent. In the case of cluster-assembled nano-structured carbon β is ~0.7.[37] The thickness and roughness values of the two nanostructured carbon samples analyzed in this work are also reported in Table 1. In particular, we deposited a cluster-assembled carbon thin film in sub-monolayer regime (SMP1) in which the coverage of the silicon substrate is not complete, as is characterized by SEM images later on in Figure 5a, and another carbon cluster-assembled thin film (SMP2), in which the porous carbon cluster-assembled thin film covers all the surface of the substrate.

In Figure 1b, the AFM morphological map of SMP2 highlights the typical rough interface of the nanostructured carbon thin film, in spite of its low thickness. The distribution of the pore radius, evaluated by gas adsorption measurements and reported in Figure 1c, shows the presence of nano- and mesopores, with a maximum in the pore radius distribution at around 3.2 nm. The pores dimension should allow the $[Bmim]^+$ and $[NTf2]^-$ ions to enter into the matrix, since their corresponding hydrodynamic radii are 7.3 Å[63] and 3.7 Å[64] approximately.

Permeability of the Ionic Liquid to the Porous Carbon Structure. In order to evaluate the accessibility of the pores by the ionic liquid, we performed nitrogen adsorption measurements, according to the method explained in ref 37, on an as-deposited ns-C film (which covers a silicon substrate total area of 12 cm^2), and we repeated the measurements on the same substrates after the drop-casting of 300 μL of 1:1000 $[Bmim][NTf2]$/methanol solution. The fine topographical details and rms surface roughness remain unchanged if the carbon thin film is covered by $[Bmim]$-$[NTf2]$/methanol solution ($R_q \approx 20$ nm), as is visible in the morphological AFM maps acquired before and after the ionic liquid deposition (Figure 2a,b), and the ionic liquid impregnates the porous matrix and remains confined inside of it, even in vacuum condition, without overflowing. The ionic liquid soaks very well the nano- and mesopores, since the carbon surface area, calculated by nitrogen adsorption isotherms shown in Figure S2 (see Supporting Information),
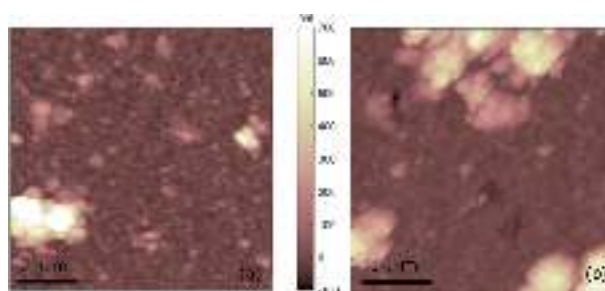

Figure 2. (a) Top-view AFM morphological map of as-deposited ns-C thin film SMP2 and (b) the same carbon sample after the deposition of 300 μL of $[Bmim][NTf2]$/methanol diluted solution onto it.

is drastically decreased (from 1550 m^2/g for as-deposited sample to 225 m^2/g after $[Bmim][NTf2]$/methanol deposition). The quantity of ionic liquid deposited is not enough to completely impregnate the nanoporous carbon matrix, since no ionic liquid appears on the upper carbon surface (Figure 2b). Otherwise, the residual specific surface area would have been even less than 225 m^2/g.

Interfacial Wettability. In the literature, the phase transition associated with fluids confined inside pores is widely discussed. For example, the shift in transition temperature, which is related to a different surface energy of the liquid with respect to the confining wall, compared to the one of the liquid in the bulk, is of great relevance for fluids of many different molecular species[65,66] and it results in the structuring and layering of the confined fluid at the interface.

Several works[20,25,46] show this structuring for confined ionic liquids, and some of them[45,67−69] describe the formation of a solid-like layer extending several tens of nanometers from the interface, depending on the properties of the solid surface. For example, the role of the ionic liquid/conductive wall surface energy for promoting the phase transition of ILs into a glassy-like state was recently demonstrated in refs 67 and 68.

In general, we can argue that if the wetting of the ionic liquid solid-phase on the walls, which is related to the surface energy of liquid−solid interface, is favored compared to the wetting of the ionic liquid in liquid phase, the phase transition of the ionic liquid into solid phase in confining conditions may occur at higher temperature than in bulk conditions. According to this consideration, we may expect that a thin film of ionic liquid that perfectly wets a surface in its liquid phase does not tend to change its structure into a solid phase.

We reported recently the absence of structured terraces on HOPG,[44] while many structured solid-like ionic liquid terraces are formed on the flat oxidized silicon surface.[44,45] For this reason, we investigated the wettability of $[Bmim][NTf2]$ on these reference substrates and on ns-C thin films. In particular, AFM allows qualitative evaluation of the wettability of $[Bmim][NTf2]$ in the liquid phase: from morphological images acquired on HOPG (Figure 3a), on flat oxidized silicon (Figure 3b), and on ns-C SMP2 (Figure 3c), the corresponding drop profiles are extracted (Figure 3d,e,f). The layers formed on the three different surfaces are exposed to air and are not covered by bulk ionic liquid: they form a sub-monolayer film on the solid substrate.

According to the AFM images, $[Bmim][NTf2]$ in the liquid phase wets HOPG substrates, while more rounded $[Bmim]$-$[NTf2]$ drops are formed on the oxidized silicon and the
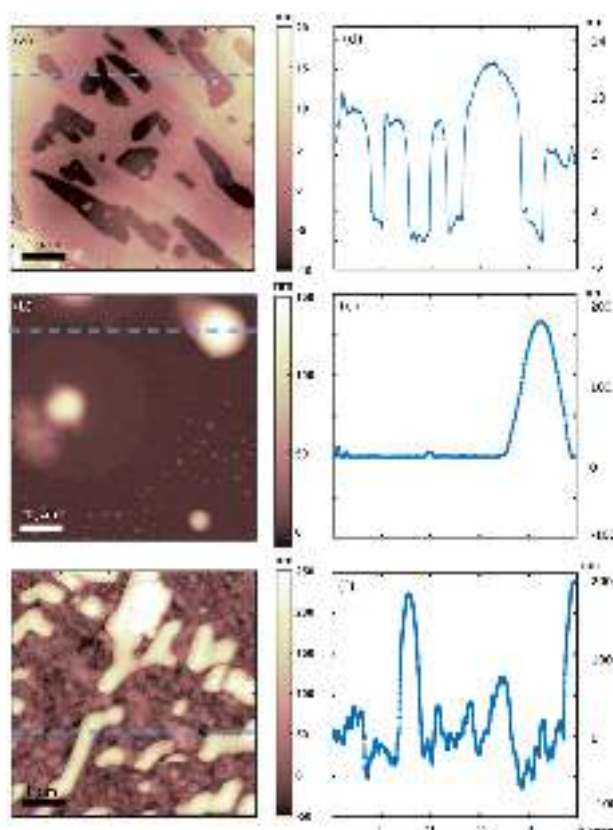
Figure 3. Top-view morphological AFM maps acquired on [Bmim]-[NTf2] deposited on HOPG (a), on a flat oxidized silicon surface (b), and on SMP2 ns-C sample (c). The light-blue dotted lines indicate the surface profiles shown on the right of each image.

Morphology of Structured [Bmim][NTf2] Terraces on ns-C Thin Films. Experiments performed in our laboratory using several different surfaces, highlighted the formation of structured solid-like [Bmim][NTf2] terraces after the drop-casting of a few microliters of diluted [Bmim][NTf2]/methanol solution. In particular, they have been observed on insulating flat substrates (mica, oxidized silicon, crystalline MgO, TiO_2, NaCl)[44,45,70] and on rough cluster assembled oxidized silica surfaces[41] produced by the low-energy cluster beam deposition in the gas phase.[36] According to the phenomenon observed, the term "solid-like" does not refer to an interfacial ordering of the ionic liquid, as is observed for the solvation layers of liquid at solid surfaces;[46,47] it concerns a transition, which implies the change of many structural and functional properties of the ionic liquid. In particular, we refer to ionic liquid multilayered micrometer-wide terraces, characterized by a 0.6 nm high[71] fundamental step, which extend from the surface up to several tens or even hundreds of nanometers.[41,44,45] The electrical properties of the solid-like structures produced in our laboratories are highly resilient to intense electric fields and possess an electrically insulating character.[45] Experimental evidence[41,45] suggests that these [Bmim][NTf$_2$] structures possess a mechanical resistance to compressive stresses that is typical of solid materials.

The deposition of 10 μL of [Bmim][NTf2]/methanol diluted solution by drop-casting onto the sub-monolayer ns-C SMP1 film reproduces structured terraces of the ionic liquid shown in Figure 4, which are similar in morphology to the ones obtained on oxidized silicon nanostructured thin film.[41] The structured ionic liquid reproduces the mesoscopic morphology of the cluster-assembled carbon surface; nevertheless, it organizes into a step-like structure as underlined by the curved edges indicated by the black narrows in the 3D AFM representation of the structured ionic liquid shown in Figure 4f, which stress the perimeters of the terraces.

The ionic liquid terraces are surrounded by a thin layer of ionic liquid in its liquid phase (thickness ~50 nm), as is shown in the AFM morphological and phase maps in Figure 4d,e.

These results represent the first experimental evidence of the interfacial structuring of ionic liquids into micrometer large and several tens of nanometers high terraces onto a conductive rough and porous carbon surface. In the phase map, shown in Figure 4e, and in the corresponding 3D AFM representation (Figure 4f), the layers constituting the structured ionic liquid terraces, characterized by wavy irregular borders, are more distinguishable. SEM images, shown in Figure 5, acquired on the as-deposited SMP1 (Figure 5a,c,e) and on the same carbon sample after drop-casting of [Bmim][NTf2]/methanol diluted solution (Figure 5b,d,f), allow one to qualitatively appreciate the different morphologies, as well as the density of the structured ionic liquid objects on the nanostructured carbon surface. The as-deposited carbon thin films are characterized by a porous morphology, which is particularly evident in the highest carbon asperities and agglomeration on the substrate, while the nanostructured carbon sample covered by the ionic liquid shows more terraced morphologies and locally smooth steps characterized by a small tilt with respect to the silicon substrate. By analyzing the SEM images acquired with low magnification, according to the strategy explained in the Supporting Information, the percentage of the ionic liquid structured into terraces surrounded by the liquid phase is 18%.

SEM images reveal also a different contrast between the liquid and the structured phase of the ionic liquid covering the
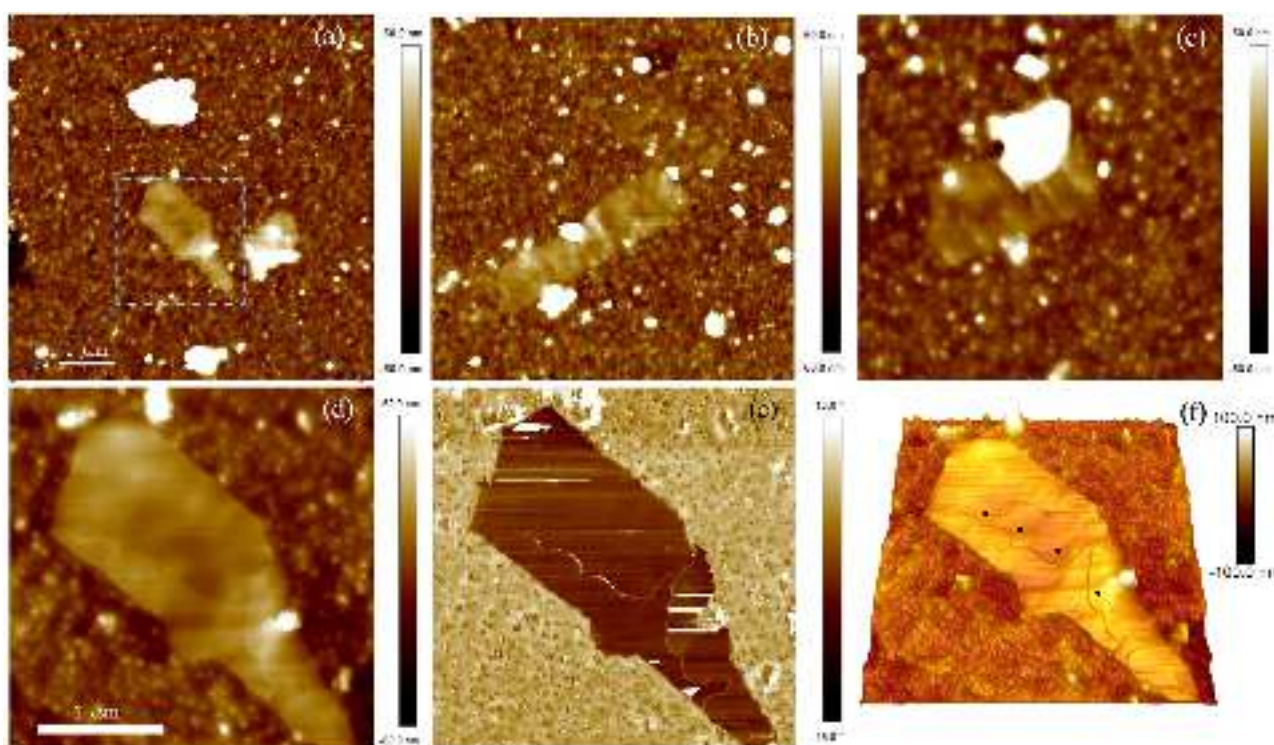
nanostructured carbon substrates. The apparent contact angle was evaluated by analyzing about ten profiles, acquired perpendicular to each drop, extracted from AFM images. In particular, the apparent contact angles between the liquid [Bmim][NTf2] and the flat oxidized silicon and SMP2 ns-C sample are 42° ± 4° and 77° ± 2°, respectively. In the case of HOPG, [Bmim][NTf2] forms a several nanometer high layer that extends discontinuously on the entire surface. Even if the ionic liquid does not form a monatomic wetting layer, since surface is not completely covered and since the height of the wetting ionic liquid layer exceeds a single molecular layer, the ionic liquid does not form isolated rounded droplets and it spreads on HOPG.

The quantity of ionic liquid deposited on the surfaces is the same for all the samples, and the resulting wetting behavior of the IL deposited in air on three different surfaces can be compared.

In particular, these results reinforce the hypothesis that the transition of ionic liquid into a solid-like phase (as in the case of flat oxidized silicon substrate) is correlated to a higher surface energy and hence a lower wettability of the liquid phase compared to the solid one, if we suppose that the surface energies of HOPG/air and of ns-C/air are comparable. Since the nanostructured carbon thin film increases the contact angle of the liquid phase of the ionic liquid, it is probable that a local solid-like ionic liquid transition takes place also on the nanostructured carbon interface.

Figure 4. (a–c) AFM morphological maps of a ns-C thin film (SMP1) covered by 10 μL of [Bmim][NTf2]/methanol solution; structured [Bmim][NTf2] surrounded by its liquid phase is demonstrated. Panels d–f show the AFM top-view, phase map, and 3D reconstruction of the structured ionic liquid shown in panel a.
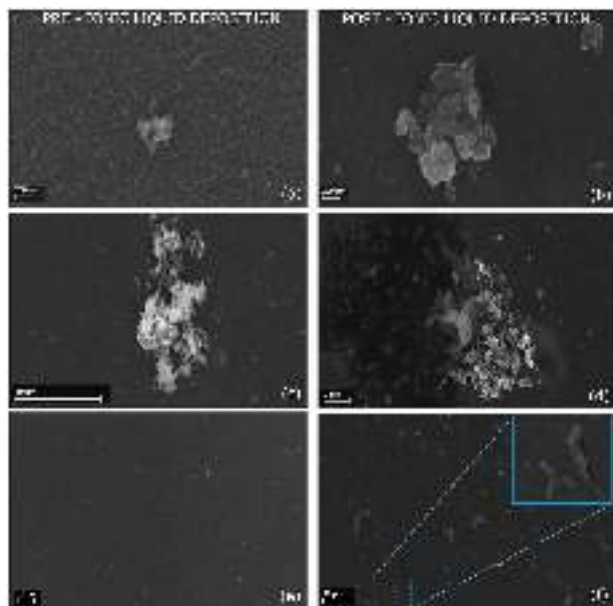

Figure 5. (a, c, e) SEM images acquired on the as-deposited ns-C thin film (SMP1) at different magnifications. (b, d, f) SEM images of SMP1 sample covered by 10 μL of [Bmim][NTf2]/methanol diluted solution. The inset of panel f shows magnified structured ionic liquid terraces grown on the nanostructured carbon surface.

carbon nanostructure, thanks to which we have calculated the percentage of structured ionic liquid covering the surface. It is not straightforward to ascribe such a lighter contrast of the structured ionic liquid objects to a less conductive behavior (that could be principally due to charge accumulation), as in the case of [Bmim][NTf2] deposited on the flat oxidized silicon substrate,[45] since a lighter contrast in SEM images is generally promoted also by an increased height of the sample. However, a different electrical behavior (a more insulating one) could be attributed to objects like the ones shown in the inset of Figure 5f. In these cases, the flat ionic liquid terraces, such as the ones shown in Figure 4, are at the same height of the highest carbon cluster asperities, which characterize the fine homogeneous morphology. A lighter contrast of these objects in SEM images can be dubiously attributed to their height, while it could be an indication of their less conductive nature. Further experiments have to be performed in order to test the structured ionic liquid terrace electrical behavior, also by AFM local capacitance spectroscopy.[45]

The drop-cast deposition of 10 μL of [Bmim][NTf2]/ methanol diluted solution onto ns-C SMP2 sample, whose morphological properties are reported in Table 1, results in the diffusion of the majority of the deposited ionic liquid into the carbon porous matrix, with the structured ionic liquid terraces remaining on the upper surface, as shown in AFM morphological and corresponding amplitude error images shown in Figure 6. Even for this sample, the height profiles shown in the insets of the images suggest that the structured ionic liquids reproduce the overall morphology of the cluster-assembled carbon surface: they are not parallel with the silicon surface following the roughening of the carbon thin film. Nevertheless, they organize into step-like morphology as shown by the sudden sharp increase of the height, which is also highlighted by the discontinuity in the amplitude error maps (Figure 6b,d,f), which stress the edges of the terraces. Also the
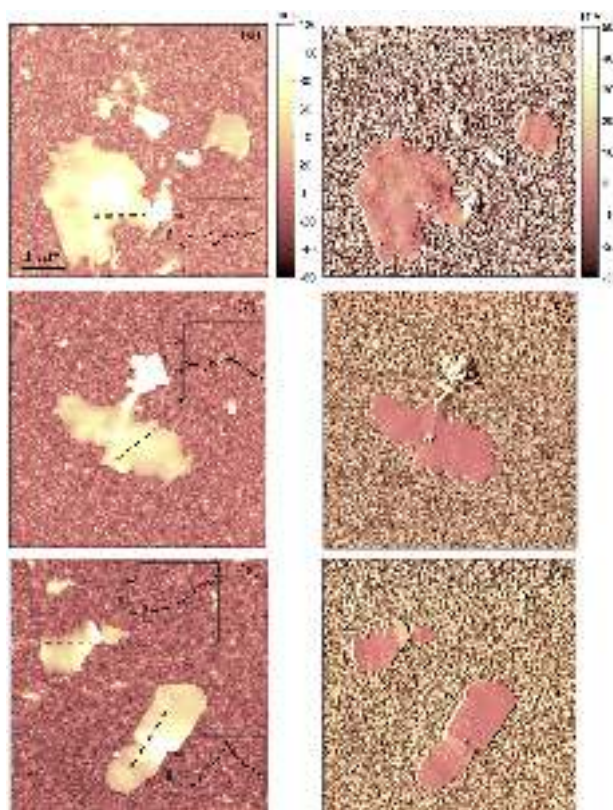
1297

Figure 6. Top-view AFM morphological images (a, c, e) and the corresponding amplitude error maps (b, d, f) of a SMP2 ns-C surface after the deposition of 10 μL of 1:1000 [Bmim][NTf2]/methanol diluted solution. The height profiles of the black dashed lines are displayed as insets of the images in panels a, c, and e.

amplitude error maps acquired by AFM help to visualize the layers that compose the structured ionic liquid terraces.

It is not clear whether the IL terraces form on the bottom of the nanostructured carbon thin film, only 150 nm thick, and propagate up to the open interface or if they structure on the upper rough carbon surface because of local morphological

curvatures and local favorable energetic conditions offered by the interactions with the carbon surface.

The possibility to study and distinguish the relative quantity of ionic liquid that penetrates the porous matrix and the portion that remains on the upper interface and also their chemical equilibrium according to the quantity of IL deposited is of fundamental importance for future developments.

Solid-like Mechanical Properties of Ionic Liquid Terraces Grown on ns-C Surfaces. Figure 7 shows the force curves acquired on structured ionic liquid terraces formed on SMP1 sample (a), on SMP2 sample (b), and the corresponding apparent Young's modulus (c). In the inset of each image, the distribution of the forces that correspond to those of the breakthrough events are reported.

The force curves acquired on the as-deposited ns-C thin films (see Figure S4 in the Supporting Information) show surface rupture events that happen on the as-deposited carbon thin films, which correspond to the compression of the local cluster-assembled carbon porous matrix. In particular, the breaks related to the nanostructured cluster-assembled thin film compression correspond to a very broad force peak in the distribution of the breakthrough forces, which appear at 263 ± 90 nN, only for the SMP2 carbon thin film. SMP1 sample shows uncorrelated rupture events of the nanostructure due to the very low thickness of the sub-monolayer carbon thin film.

Differently, the rupture events of the structured ionic liquid terraces (Figure 7a,b) correspond to sharp breakthrough force peaks in the force distribution, appearing at highest forces for SMP2 compared to SMP1 sample; in particular, they are 63 ± 20 nN for SMP1, while 107 ± 3 nN and 165 ± 29 nN for SMP2. The third peak in the force distribution shown in Figure 7b ($F = 240 \pm 16$ nN) could be attributed the rupture of the carbon nanostructure.

Accordingly, the apparent Young's modulus of the structured ionic liquid terraces (whose distribution is reported in Figure 7c), calculated by analyzing the force indentation curves with the Hertz contact mechanical model,[58] is slightly higher for SMP2 compared to SMP1. In particular, the median value and the standard deviation of the apparent Young's modulus are 0.4 ± 0.1 GPa and 0.7 ± 0.1 GPa for SMP1 and SMP2. Both the apparent Young's modulus values confirm the solid character of the structured ionic liquid terraces formed on
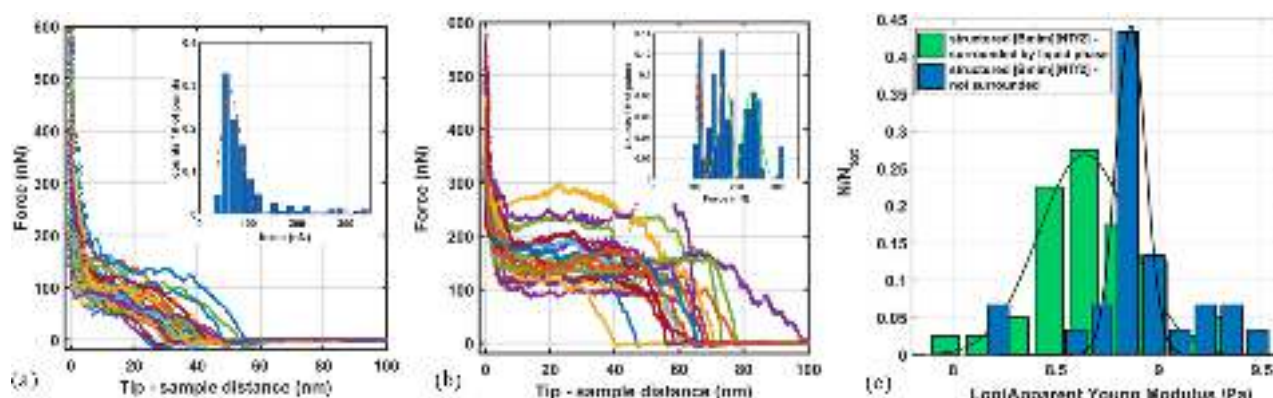

Figure 7. Force curves acquired on structured [Bmim][NTf2] covering SMP1 sample (a) and SMP2 ns-C sample (b) and the corresponding distribution of the logarithmic values of the apparent Young's modulus calculated from the force curves, SMP1 in green and SMP2 in blue (c). A Gaussian fit is superimposed on the experimental data for each distribution. The centers of the Gaussian distributions are 0.4 ± 0.1 GPa for SMP1 and 0.7 ± 0.1 GPa for SMP2. In the insets of images a and b, the distributions of the force corresponding to the rupture events in the force curves are shown.

nanostructured carbon thin films. They are in good agreement also with the apparent Young's modulus of solid-like islands formed on flat oxidized silicon substrate.[45] The nanostructure does not prevent the formation of structured ionic liquid domains, whose solid-like behavior is experimentally provided.

The small discrepancy between the solid-like ionic liquid terraces on the two different carbon samples can be conferred to the metastable state of these solid-like objects at room temperature; if they coexist with surrounding liquid phase on the nanostructured carbon thin films, as in the case of SMP1, their mechanical properties could be affected by the perturbation promoted by the liquid phase. Anyway, a larger discrepancy results between apparent Young's modulus values of structured solid-like terraced formed on nanostructured carbon thin films and the ones grown on nanostructured oxidized silicon surface,[41] which was around 60 MPa.

The conductive nature of the nanostructured carbon thin film may play a crucial role in providing more suitable energetic conditions to the disordered nanostructured matrix/ [Bmim][NTf2] interface than the insulating nanostructured oxidized silicon surface. Further experiments enabling us to discern between the contribution of the morphology and the role of the electrical properties of the supporting porous matrix in the formation of such solid-like ionic liquid structures will be deeply performed in the next future.

Imaging of Ionic Liquid Solid-like Terraces Lying beneath a Large Amount of ILs. In the majority of sensors and electrochemical applications,[21,72,73] several hundreds of microliters of pure ionic liquid are deposited at the interface of a flat or nanostructured porous solid surface. This means that over the first hundreds of nanometers from the ionic liquid/ surface interface, there are at least several micrometers of ionic liquid in its bulk phase. The stability of the structured solid-like ionic liquid terraces, which up to now have been characterized for a very thin layer of ionic liquid (100 nm), cannot be assumed. For this reason, we deposited 10 μL of 5:1000 [Bmim][NTf2]/methanol diluted solution on an as-deposited ns-C thin film, with the same morphological properties of SMP2, which form approximately a 1 μm high layer of ionic liquid in its bulk phase.

By acquisition of images in tapping mode (Figure 8a,b), as was done for the previous samples, it was not possible to identify the asperities of the morphology that emerge from the layer of the ionic liquid and discern if they belong to the nanostructured carbon surface local morphology or to the ionic liquid structured on the carbon surface. The triangular shape of the object in Figure 8b suggests that the latter hypothesis is true, but it is not undeniable. By use of a different imaging mode (peak-force tapping (PFT) mode, as explained in Materials and Methods section), it was possible to penetrate the relatively thick bulk of ionic liquid and image the underlying nanostructured carbon film. The morphological map (Figure 8c) acquired in PFT mode accurately reproduces the rough surface of the carbon morphology very well. The contrast associated with the simultaneously acquired Inphase map (Figure 8d), which considers the dissipative interaction between the AFM tip and the carbon sample, does not show any qualitative different signal coming from the highest asperities of the carbon rough surface. In contrast, morphologically smooth ionic liquid domains (Figure 8e,g), evidenced with light-blue circles in Figure 8e, and the height profile are not ascribable to carbon film morphology because of their regular and smooth micrometer large surfaces, and because
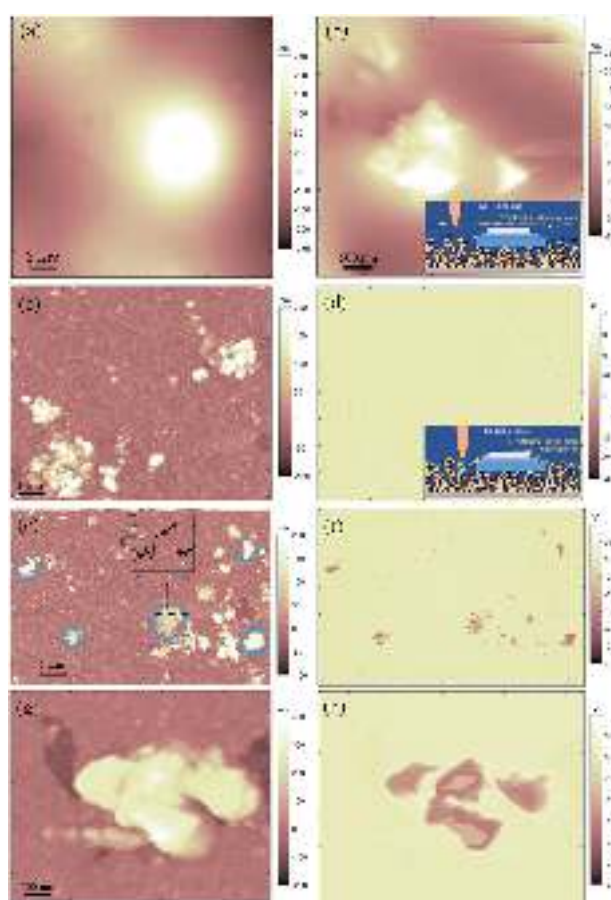

Figure 8. (a, b) Top-view AFM morphological maps of 150 nm thick ns-C thin film covered by 10 μL of 5:1000 [Bmim][NTf2]/methanol diluted solution acquired in tapping mode. (c, e, g) Morphological maps acquired on the same sample in peak-force tapping mode and the corresponding Inphase maps (d, f, h). The insets of panels b and d offer schematic descriptions of the different AFM imaging modes.

they show a remarkable contrast in the Inphase maps (Figure 8f,h) that highlight a difference in the chemical composition of the lightest (nanostructured carbon) and darkest (structured ionic liquid) regions. Solid-like [Bmim][NTf2] terraces not only formed on the carbon nanostructured thin film, but they also remain intact even below a considerable amount of ionic liquid in its bulk phase.

Effects of Ionic Liquid Confinement on Porous Carbon Electrodes. In the specific case of electrochemical and energy storage/conversion devices,[38,39,74] the formation and the stability of solid-like domains of ionic liquid at the interface with the nanostructured carbon porous matrix could prevent the double layer organization of the ionic liquid close to the electrified interface and hence prevent the most effective operation mode of the electrochemical device. In order to characterize any possible influence of the solid-like IL domains formed at the interface with the nanostructured carbon thin film on the double layer capacitance, we realized planar supercapacitors according to the method explained in ref 38 (see also Materials and Method). In particular, we filled the gap between the nanostructured electrodes of a nanoporous carbon-based supercapacitor by the deposition of 300 μL of pure [Bmim][NTf2], while on another supercapacitor (morphologically identical to the first one) 10 μL of

[Bmim][NTf2]/methanol diluted solution was previously drop-cast and then covered by 300 μL of pure [Bmim][NTf2].

The cyclic voltammetry curves, reported in Figure 9a, show a regular rectangular shape between −500 mV and 500 mV, which indicates a capacitive electrode response and the lack of faradaic reactions on the surface. The interfacial electrical double layer capacitances, calculated from electrochemical impedance spectroscopy measurements (two representative curves are reported in Figure 9b) at 0.01 Hz with[75] $C(f) = -Z'(f)/(2\pi f |Z(f)|^2)$, where f is the frequency, Z' and Z are the imaginary and real parts of the impedance, are 0.2 ± 0.01 mF/cm^2 for a supercapacitor composed of bulk ionic liquid, which is comparable to results shown in literature,[38] and 0.15 ± 0.01 mF/cm^2 for the supercapacitor with the preformed solid-like ionic liquid terraces. Each measurement was performed on 5 samples with identical morphological properties.

Electrochemical impedance spectroscopy (EIS) results are of great interest because they provide evidence of the persistence of local solid-like ionic liquid domains on the nanostructured carbon surface, which due to their mechanical properties do not allow a complete reorganization of the ionic liquid into a double-layer structure, even if they are covered by a huge amount of bulk ionic liquid. The mean decrease of 20% in the value of the specific surface capacitance, far from the discrepancy associated with the measurements (which is 5%, by considering the 5 replicated samples), can be barely justified by the presence of solid-like domains only on the upper nanostructured interface; the formation of such solid ionic liquid terraces inside the porous carbon matrix can be supposed. Interestingly, the percentage decrease of the specific surface capacitance corresponds to the same percentage of coverage of the ionic liquid structured into terraces on SMP1, characterized by the SEM images as shown before.

The decrease in specific surface capacitance is also associated with a decrease in the so-called solution resistance of about 20% (calculated by the replicated samples), which refers to the real part of the impedance at high frequency, which is highlighted in Figure 9c in the Nyquist plot. The very low mobility of solid-like terraces should increase the resistance of the system instead of decreasing it. Two phenomena can cooperate to promote this unexpected result: first of all the insertion of confined ionic liquid inside the porous carbon matrix can improve the carbon conductivity by compensating carbon defects.[76] In the literature, it has been computationally demonstrated that the adsorption of ionic liquid ([Bmim][NTf2] specifically) on a carbon interface characterized by different kinds of defects can decrease the Fermi energy level and improve the conductivity of the thin film.[76] For this reason, a thin film of ionic liquid can act as an interlayer component for the suppression of side reactions on supercapacitors and batteries based on carbonaceous materials.[77] Second, the possible lower permeability of the ionic liquid to the carbon nanostructured matrix due to the formation of the solid-like terraces inside the porous matrix, could also influence the resistance of the porous carbon material due to the local absence of the electrolyte close to the carbon interface. This interesting result has to be further investigated, in particular by studying the electrical and ionic conductivity of nanostructured carbon/ionic liquid interface in electrical and electrochemical systems with different complexity (from simple electrically conductive path[78] to electrolyte gated transistor[74]).
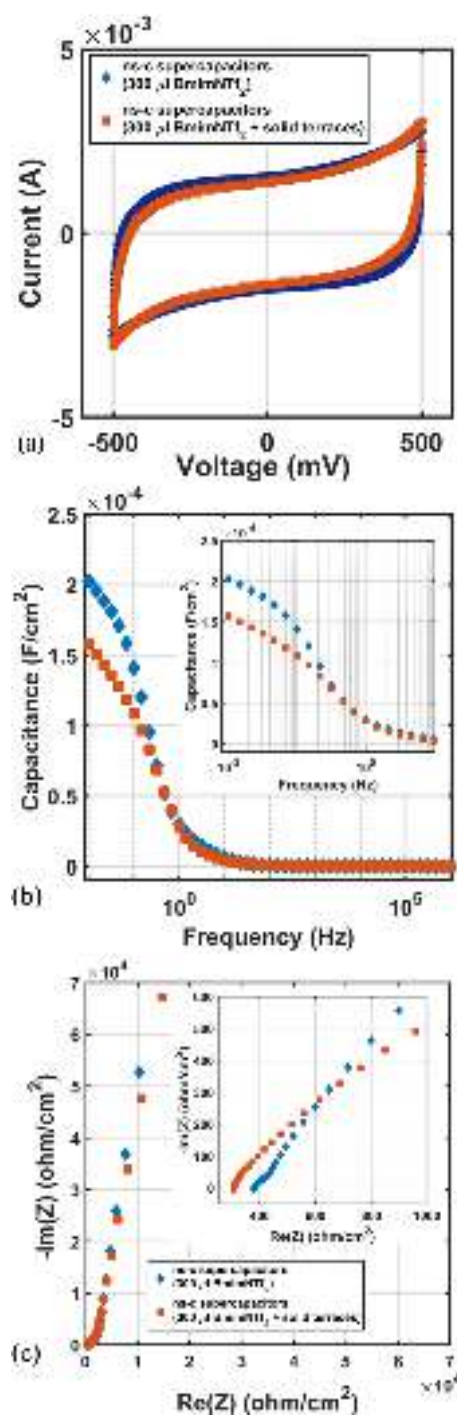

Figure 9. Cyclic voltammetry (a) and electrochemical impedance spectroscopy curves (b) acquired on a planar supercapacitor based on 150 nm thick ns-C nanostructured electrodes and 300 μL of [Bmim][NTf2] with and without previously induced solid-like IL terraces on the carbon interface, according to the drop-casting method explained in this work; a comparison between the Nyquist plots acquired on the two supercapacitors are shown in panel c, with an inset highlighting the high frequency response.

■ CONCLUSIONS

This work provides the first experimental evidence of the structuring of the ionic liquid [Bmim][NTf2] into solid-like

terraces at the interface with nanoporous cluster-assembled carbon thin films. The characterization of the mechanical properties of the structured IL confirms that the disordered surface carbon morphology does not prevent the formation of stable and strong ionic interactions close to the surface, which confer to the structured IL a solid-like character. The morphological properties and the conductive nature of the nanostructured carbon matrix provide the surface energetic boundary conditions, as shown also by the IL wettability behavior, which promote the solid-like structuring.

Our results provide robust evidence of the dependence of the macroscopic response of a planar supercapacitor, based on ns-C thin films and IL, on the local formation of structured solid-like ionic liquid inside the nanoporous matrix of the carbon electrodes. In particular, the effect of the ionic liquid transition locally formed on the nanostructured surface is relevant to the capacitance of the planar nanostructured supercapacitor. These results suggest that the phenomena characterized at the upper carbon thin film interface by AFM can happen also inside the porous matrix.

It would be interesting to repeat similar characterization when the sample is not only produced but also characterized in a nitrogen controlled atmosphere. The presence of water in the samples, which depends on how long they are exposed to air and the relative humidity, could affect the stability of the structured ionic liquid because of its hygroscopic properties.[79]

The decrease of the carbon thin film resistance due to the insertion of confined ionic liquid inside the porous carbon matrix, interacting with carbon film defects, can be ascribed to the confinement of a tiny amount of ionic liquid inside the porous structure and not directly to the formation of the solid-like ionic liquid domains. Its relevance for the performance of electrochemical devices is very important from the technological point of view, and it demands further characterization, through the combined approach of local imaging techniques and electrochemical measurements, in order to understand and control the behavior of the confined ionic liquid inside the bulk of the porous carbon thin film.

ASSOCIATED CONTENT

Supporting Information

The Supporting Information is available free of charge at https://pubs.acs.org/doi/10.1021/acs.jpcc.0c08145.

Deposition of evaporated gold and nanostructured carbon for supercapacitor, nitrogen adsorption isotherms, evaluation of the coverage of the structured ionic liquid on ns-C thin film, and force spectroscopy on ns-C thin films (PDF)

AUTHOR INFORMATION

Corresponding Authors

Francesca Borghi − CIMaINa and Dipartimento di Fisica "Aldo Pontremoli", Università degli Studi di Milano, 20133 Milano, Italy; ● orcid.org/0000-0001-6980-4910; Email: francesca.borghi@unimi.it

Alessandro Podestà − CIMaINa and Dipartimento di Fisica "Aldo Pontremoli", Università degli Studi di Milano, 20133 Milano, Italy; ● orcid.org/0000-0002-4169-6679; Email: alessandro.podesta@mi.infn.it

Authors

Claudio Piazzoni − CIMaINa and Dipartimento di Fisica "Aldo Pontremoli", Università degli Studi di Milano, 20133 Milano, Italy

Matteo Ghidelli − Laboratoire des Sciences des Procédés et des Matériaux (LSPM), CNRS, Université Sorbonne Paris Nord, 93430 Villetaneuse, France

Paolo Milani − CIMaINa and Dipartimento di Fisica "Aldo Pontremoli", Università degli Studi di Milano, 20133 Milano, Italy

Complete contact information is available at:
https://pubs.acs.org/10.1021/acs.jpcc.0c08145

Notes

The authors declare no competing financial interest.

REFERENCES

(1) Kim, B. C.; Hong, J.-Y.; Wallace, G. G.; Park, H. S. Recent Progress in Flexible Electrochemical Capacitors: Electrode Materials, Device Configuration, and Functions. *Adv. Energy Mater.* **2015**, 5 (22), 1500959.

(2) Chen, Y.; Zhang, Y.; Liang, Z.; Cao, Y.; Han, Z.; Feng, X. Flexible Inorganic Bioelectronics. *npj Flexible Electronics* **2020**, 4, 2.

(3) He, Y.; Chen, W.; Gao, C.; Zhou, J.; Li, X.; Xie, E. An Overview of Carbon Materials for Flexible Electrochemical Capacitors. *Nanoscale* **2013**, 5 (19), 8799.

(4) Shao, H.; Wu, Y.-C.; Lin, Z.; Taberna, P.-L.; Simon, P. Nanoporous Carbon for Electrochemical Capacitive Energy Storage. *Chem. Soc. Rev.* **2020**, 49 (10), 3005−3039.

(5) Chen, G. Z. Supercapacitor and Supercapattery as Emerging Electrochemical Energy Stores. *Int. Mater. Rev.* **2017**, 62 (4), 173−202.

(6) Soavi, F.; Bettini, L. G.; Piseri, P.; Milani, P.; Santoro, C.; Atanassov, P.; Arbizzani, C. Miniaturized Supercapacitors: Key Materials and Structures towards Autonomous and Sustainable Devices and Systems. *J. Power Sources* **2016**, 326, 717−725.

(7) Snook, G. A.; Kao, P.; Best, A. S. Conducting-Polymer-Based Supercapacitor Devices and Electrodes. *J. Power Sources* **2011**, 196 (1), 1−12.

(8) Liang, J.; Jiang, C.; Wu, W. Toward Fiber-, Paper-, and Foam-Based Flexible Solid-State Supercapacitors: Electrode Materials and Device Designs. *Nanoscale* **2019**, 11 (15), 7041−7061.

(9) Pandolfo, A. G.; Hollenkamp, A. F. Carbon Properties and Their Role in Supercapacitors. *J. Power Sources* **2006**, 157 (1), 11−27.

(10) Merlet, C.; Rotenberg, B.; Madden, P. A.; Taberna, P.-L.; Simon, P.; Gogotsi, Y.; Salanne, M. On the Molecular Origin of Supercapacitance in Nanoporous Carbon Electrodes. *Nat. Mater.* **2012**, 11 (4), 306−310.

(11) Wang, G.; Zhang, L.; Zhang, J. A Review of Electrode Materials for Electrochemical Supercapacitors. *Chem. Soc. Rev.* **2012**, 41 (2), 797−828.

(12) Zhai, Y.; Dou, Y.; Zhao, D.; Fulvio, P. F.; Mayes, R. T.; Dai, S. Carbon Materials for Chemical Capacitive Energy Storage. *Adv. Mater.* **2011**, 23 (42), 4828−4850.

(13) Balducci, A.; Dugas, R.; Taberna, P. L.; Simon, P.; Plée, D.; Mastragostino, M.; Passerini, S. High Temperature Carbon-carbon Supercapacitor Using Ionic Liquid as Electrolyte. *J. Power Sources* **2007**, 165 (2), 922−927.

(14) Torop, J.; Palmre, V.; Arulepp, M.; Sugino, T.; Asaka, K.; Aabloo, A. Flexible Supercapacitor-like Actuator with Carbide-Derived Carbon Electrodes. *Carbon* **2011**, *49* (9), 3113−3119.

(15) Zhang, L. L.; Zhao, X. S. Carbon-Based Materials as Supercapacitor Electrodes. *Chem. Soc. Rev.* **2009**, *38* (9), 2520.

(16) Beal, J. M. Surgical Grand Rounds: Ruptured Abdominal Aortic Aneurysm. *IMJ. Ill Med. J.* **1975**, *148* (5), 516−518.

(17) Simon, P.; Gogotsi, Y. Materials for Electrochemical Capacitors. *Nat. Mater.* **2008**, *7* (11), 845−854.

(18) Zhang, S.; Zhang, J.; Zhang, Y.; Deng, Y. Nanoconfined Ionic Liquids. *Chem. Rev.* **2017**, *117* (10), 6755−6833.

(19) Borghi, F.; Podestà, A. Ionic Liquids under Nanoscale Confinement. *Advances in Physics: X* **2020**, *5* (1), 1736949.

(20) Perkin, S. Ionic Liquids in Confined Geometries. *Phys. Chem. Chem. Phys.* **2012**, *14* (15), 5052−5062.

(21) Singh, M. P.; Singh, R. K.; Chandra, S. Ionic Liquids Confined in Porous Matrices: Physicochemical Properties and Applications. *Prog. Mater. Sci.* **2014**, *64*, 73−120.

(22) Im, J.; Cho, S. D.; Kim, M. H.; Jung, Y. M.; Kim, H. S.; Park, H. S. Anomalous Thermal Transition and Crystallization of Ionic Liquids Confined in Graphene Multilayers. *Chem. Commun.* **2012**, *48* (14), 2015−2017.

(23) Chen, S.; Wu, G.; Sha, M.; Huang, S. Transition of Ionic Liquid [Bmim][PF6] from Liquid to High-Melting-Point Crystal When Confined in Multiwalled Carbon Nanotubes. *J. Am. Chem. Soc.* **2007**, *129*, 2416.

(24) Rajput, N. N.; Monk, J.; Hung, F. R. Structure and Dynamics of an Ionic Liquid Confined Inside a Charged Slit Graphitic Nanopore. *J. Phys. Chem. C* **2012**, *116* (27), 14504−14513.

(25) Lahrar, E. H.; Belhboub, A.; Simon, P.; Merlet, C. Ionic Liquids under Confinement: From Systematic Variations of the Ion and Pore Sizes toward an Understanding of the Structure and Dynamics in Complex Porous Carbons. *ACS Appl. Mater. Interfaces* **2020**, *12* (1), 1789−1798.

(26) Ghoufi, A.; Szymczyk, A.; Malfreyt, P. Ultrafast Diffusion of Ionic Liquids Confined in Carbon Nanotubes. *Sci. Rep.* **2016**, *6* (April), 1−9.

(27) Chathoth, S. M.; Mamontov, E.; Dai, S.; Wang, X.; Fulvio, P. F.; Wesolowski, D. J. Fast Diffusion in a Room Temperature Ionic Liquid Confined in Mesoporous Carbon. *Epl* **2012**, *97* (6), 66004.

(28) Merz, S.; Jakes, P.; Taranenko, S.; Eichel, R. A.; Granwehr, J. Dynamics of [Pyr13][Tf2N] Ionic Liquid Confined to Carbon Black. *Phys. Chem. Chem. Phys.* **2019**, *21* (31), 17018−17028.

(29) Feng, G.; Huang, J.; Sumpter, B. G.; Meunier, V.; Qiao, R. A "Counter-Charge Layer in Generalized Solvents" Framework for Electrical Double Layers in Neat and Hybrid Ionic Liquid Electrolytes. *Phys. Chem. Chem. Phys.* **2011**, *13* (32), 14723−14734.

(30) Bazant, M. Z.; Storey, B. D.; Kornyshev, A. A. Double Layer in Ionic Liquids: Overscreening versus Crowding. *Phys. Rev. Lett.* **2011**, *106* (4), 6−9.

(31) Kondrat, S.; Kornyshev, A. Erratum: Superionic State in Double-Layer Capacitors with Nanoporous Electrodes (J. Phys.: Condens. Matter (2011) 23 (022201)). *J. Phys.: Condens. Matter* **2013**, *25* (11), 119501.

(32) Futamura, R.; Iiyama, T.; Takasaki, Y.; Gogotsi, Y.; Biggs, M. J.; Salanne, M.; Ségalini, J.; Simon, P.; Kaneko, K. Partial Breaking of the Coulombic Ordering of Ionic Liquids Confined in Carbon Nanopores. *Nat. Mater.* **2017**, *16* (12), 1225−1232.

(33) Sheehan, A.; Jurado, L. A.; Ramakrishna, S. N.; Arcifa, A.; Rossi, A.; Spencer, N. D.; Espinosa-Marzal, R. M. Layering of Ionic Liquids on Rough Surfaces. *Nanoscale* **2016**, *8* (7), 4094−4106.

(34) An, R.; Zhu, Y.; Wu, N.; Xie, W.; Lu, J.; Feng, X.; Lu, X. Wetting Behavior of Ionic Liquid on Mesoporous Titanium Dioxide Surface by Atomic Force Microscopy. *ACS Appl. Mater. Interfaces* **2013**, *5* (7), 2692−2698.

(35) Rajput, N. N.; Monk, J.; Hung, F. R. Ionic Liquids Confined in a Realistic Activated Carbon Model: A Molecular Simulation Study. *J. Phys. Chem. C* **2014**, *118* (3), 1540−1553.

(36) Wegner, K.; Piseri, P.; Tafreshi, H. V.; Milani, P. Cluster Beam Deposition: A Tool for Nanoscale Science and Technology. *J. Phys. D: Appl. Phys.* **2006**, *39* (22), R439−R459.

(37) Borghi, F.; Milani, M.; Bettini, L. G.; Podestà, A.; Milani, P. Quantitative Characterization of the Interfacial Morphology and Bulk Porosity of Nanoporous Cluster-Assembled Carbon Thin Films. *Appl. Surf. Sci.* **2019**, *479*, 395−402.

(38) Bettini, L. G.; Galluzzi, M.; Podestà, A.; Milani, P.; Piseri, P. Planar Thin Film Supercapacitor Based on Cluster-Assembled Nanostructured Carbon and Ionic Liquid Electrolyte. *Carbon* **2013**, *59*, 212−220.

(39) Yi, Z.; Bettini, L. G.; Tomasello, G.; Kumar, P.; Piseri, P.; Valitova, I.; Milani, P.; Soavi, F.; Cicoira, F. Flexible Conducting Polymer Transistors with Supercapacitor Function. *J. Polym. Sci., Part B: Polym. Phys.* **2017**, *55* (1), 96−103.

(40) Bettini, L. G.; Bellacicca, A.; Piseri, P.; Milani, P. Supersonic Cluster Beam Printing of Carbon Microsupercapacitors on Paper. *Flexible and Printed Electronics* **2017**, *2* (2), 025002.

(41) Borghi, F.; Milani, P.; Podestà, A. Solid-Like Ordering of Imidazolium-Based Ionic Liquids at Rough Nanostructured Oxidized Silicon Surfaces. *Langmuir* **2019**, *35* (36), 11881−11890.

(42) Bruzzi, M.; Piseri, P.; Miglio, S.; Bongiorno, G.; Barborini, E.; Ducati, C.; Robertson, J.; Milani, P. Electrical Conduction in Nanostructured Carbon and Carbon-Metal Films Grown by Super-sonic Cluster Beam Deposition. *Eur. Phys. J. B* **2003**, *36* (1), 3−13.

(43) Bongiorno, G.; Podesta, A.; Ravagnan, L.; Piseri, P.; Milani, P.; Lenardi, C.; Miglio, S.; Bruzzi, M.; Ducati, C. Electronic Properties and Applications of Cluster-Assembled Carbon Films. *J. Mater. Sci.: Mater. Electron.* **2006**, *17* (6), 427−441.

(44) Bovio, S.; Podestà, A.; Lenardi, C.; Milani, P. Evidence of Extended Solidlike Layering in [Bmim][NTf2] Ionic Liquid Thin Films at Room-Temperature. *J. Phys. Chem. B* **2009**, *113* (19), 6600−6603.

(45) Galluzzi, M.; Bovio, S.; Milani, P.; Podestà, A. Surface Confinement Induces the Formation of Solid-Like Insulating Ionic Liquid Nanostructures. *J. Phys. Chem. C* **2018**, *122* (14), 7934−7944.

(46) Atkin, R.; Warr, G. G. Structure in Confined Room-Temperature Ionic Liquids. *J. Phys. Chem. C* **2007**, *111* (13), 5162−5168.

(47) Atkin, R.; El Abedin, S. Z.; Hayes, R.; Gasparotto, L. H. S.; Borisenko, N.; Endres, F. AFM and STM Studies on the Surface Interaction of [BMP]TFSA and [EMIm]TFSA Ionic Liquids with Au(111). *J. Phys. Chem. C* **2009**, *113* (30), 13266−13272.

(48) Bovio, S.; Podestà, A.; Lenardi, C.; Milani, P. Evidence of Extended Solidlike Layering in [Bmim][NTf2] Ionic Liquid Thin Films at Room-Temperature. *J. Phys. Chem. B* **2009**, *113* (19), 6600−6603.

(49) Milani, P.; Iannotta, S. *Cluster Beam Synthesis of Nanostructured Materials*; Springer: Berlin, Heidelberg, 1999.

(50) Barborini, E.; Piseri, P.; Milani, P. Pulsed Microplasma Source of High Intensity Supersonic Carbon Cluster Beams. *J. Phys. D: Appl. Phys.* **1999**, *32* (21), L105−L109.

(51) Donadio, D.; Colombo, L.; Milani, P.; Benedek, G. Growth of Nanostructured Carbon Films by Cluster Assembly. *Phys. Rev. Lett.* **1999**, *83* (4), 776−779.

(52) Bongiorno, G.; Blomqvist, M.; Piseri, P.; Milani, P.; Lenardi, C.; Ducati, C.; Caruso, T.; Rudolf, P.; Wachtmeister, S.; Csillag, S.; et al. Nanostructured CNx (0 < x < 0.2) Films Grown by Supersonic Cluster Beam Deposition. *Carbon* **2005**, *43* (7), 1460−1469.

(53) Espinosa-Marzal, R. M.; Arcifa, A.; Rossi, A.; Spencer, N. D. Ionic Liquids Confined in Hydrophilic Nanocontacts: Structure and Lubricity in the Presence of Water. *J. Phys. Chem. C* **2014**, *118* (12), 6491−6503.

(54) Sakai, K.; Okada, K.; Uka, A.; Misono, T.; Endo, T.; Sasaki, S.; Abe, M.; Sakai, H. Effects of Water on Solvation Layers of Imidazolium-Type Room Temperature Ionic Liquids on Silica and Mica. *Langmuir* **2015**, *31* (22), 6085−6091.

(55) Cui, T.; Lahiri, A.; Carstens, T.; Borisenko, N.; Pulletikurthi, G.; Kuhl, C.; Endres, F. Influence of Water on the Electrified Ionic

Liquid/Solid Interface: A Direct Observation of the Transition from a Multilayered Structure to a Double-Layer Structure. *J. Phys. Chem. C* **2016**, *120* (17), 9341−9349.

(56) Gong, X.; Kozbial, A.; Li, L. What Causes Extended Layering of Ionic Liquids on the Mica Surface? *Chemical Science* **2015**, *6* (6), 3478−3482.

(57) Podesta, A.; Borghi, F.; Indrieri, M.; Bovio, S.; Piazzoni, C.; Milani, P. Nanomanufacturing of Titania Interfaces with Controlled Structural and Functional Properties by Supersonic Cluster Beam Deposition. *J. Appl. Phys.* **2015**, *118* (23), 234309.

(58) Butt, H.-J.; Cappella, B.; Kappl, M. Force Measurements with the Atomic Force Microscope: Technique, Interpretation and Applications. *Surf. Sci. Rep.* **2005**, *59* (1−6), 1−152.

(59) Cappella, B.; Dietler, G. Force-Distance Curves by Atomic Force Microscopy. *Surf. Sci. Rep.* **1999**, *34* (1−3), 1−104.

(60) Puricelli, L.; Galluzzi, M.; Schulte, C.; Podestà, A.; Milani, P. Nanomechanical and Topographical Imaging of Living Cells by Atomic Force Microscopy with Colloidal Probes. *Rev. Sci. Instrum.* **2015**, *86* (3), 033705.

(61) Amar, J. G.; Family, F.; Lam, P.-M. Dynamic Scaling of the Island-Size Distribution and Percolation in a Model of Submonolayer Molecular-Beam Epitaxy. *Phys. Rev. B: Condens. Matter Mater. Phys.* **1994**, *50* (12), 8781−8797.

(62) Family, F.; Vicsek, T. Scaling of the Active Zone in the Eden Process on Percolation Networks and the Ballistic Deposition Model. *J. Phys. A: Math. Gen.* **1985**, *18* (2), L75−L81.

(63) Xu, Y.; Tian, Z.; Wang, S.; Wang, L.; Hou, L.; Ma, Y.; Wei, Y.; Ma, H.; Wang, B.; Xu, Z.; et al. Ionothermal Synthesis of Aluminophosphate Molecular Sieves. *Stud. Surf. Sci. Catal.* **2007**, *170*, 228−232.

(64) Voeltzel, N.; Vergne, P.; Fillot, N.; Bouscharain, N.; Joly, L. Rheology of an Ionic Liquid with Variable Carreau Exponent: A Full Picture by Molecular Simulation with Experimental Contribution. *Tribol. Lett.* **2016**, *64*, 25.

(65) Evans, R. Fluids Adsorbed in Narrow Pores: Phase Equilibria and Structure. *J. Phys.: Condens. Matter* **1990**, *2* (46), 8989−9007.

(66) Tarazona, P.; Marconi, U. M. B.; Evans, R. Phase Equilibria of Fluid Interfaces and Confined Fluids: Non-Local versus Local Density Functionals. *Mol. Phys.* **1987**, *60* (3), 573−595.

(67) Comtet, J.; Niguès, A.; Kaiser, V.; Coasne, B.; Bocquet, L.; Siria, A. Nanoscale Capillary Freezing of Ionic Liquids Confined between Metallic Interfaces and the Role of Electronic Screening. *Nat. Mater.* **2017**, *16* (6), 634−639.

(68) Lainé, A.; Niguès, A.; Bocquet, L.; Siria, A. Nanotribology of Ionic Liquids: Transition to Yielding Response in Nanometric Confinement with Metallic Surfaces. *Phys. Rev. X* **2020**, *10* (1), 1−10.

(69) Sheehan, A.; Jurado, L. A.; Ramakrishna, S. N.; Arcifa, A.; Rossi, A.; Spencer, N. D.; Espinosa-Marzal, R. M. Layering of Ionic Liquids on Rough Surfaces. *Nanoscale* **2016**, *8* (7), 4094−4106.

(70) Bovio, S.; Podesta, A.; Milani, P.; Ballone, P.; Del Popolo, M. G. Nanometric Ionic-Liquid Films on Silica: A Joint Experimental and Computational Study. *J. Phys.: Condens. Matter* **2009**, *21* (42), 424118.

(71) Ballone, P.; Del Popolo, M. G.; Bovio, S.; Podesta, A.; Milani, P.; Manini, N. Nano-Indentation of a Room-Temperature Ionic Liquid Film on Silica: A Computational Experiment. *Phys. Chem. Chem. Phys.* **2012**, *14* (7), 2475−2482.

(72) Zhang, S.; Sun, J.; Zhang, X.; Xin, J.; Miao, Q.; Wang, J. Ionic Liquid-Based Green Processes for Energy Production. *Chem. Soc. Rev.* **2014**, *43* (22), 7838−7869.

(73) Palacio, M.; Bhushan, B. A Review of Ionic Liquids for Green Molecular Lubrication in Nanotechnology. *Tribol. Lett.* **2010**, *40* (2), 247−268.

(74) Sayago, J.; Meng, X.; Quenneville, F.; Liang, S.; Bourbeau, É.; Soavi, F.; Cicoira, F.; Santato, C. Electrolyte-Gated Polymer Thin Film Transistors Making Use of Ionic Liquids and Ionic Liquid-Solvent Mixtures. *J. Appl. Phys.* **2015**, *117* (11), 112809.

(75) Taberna, P. L.; Simon, P.; Fauvarque, J. F. Electrochemical Characteristics and Impedance Spectroscopy Studies of Carbon-Carbon Supercapacitors. *J. Electrochem. Soc.* **2003**, *150* (3), A292.

(76) Shakourian-Fard, M.; Kamath, G. The Effect of Defect Types on the Electronic and Optical Properties of Graphene Nanoflakes Physisorbed by Ionic Liquids. *Phys. Chem. Chem. Phys.* **2017**, *19* (6), 4383−4395.

(77) Lou, P.; Li, C.; Cui, Z.; Guo, X. Job-Sharing Cathode Design for Li-O$_2$ Batteries with High Energy Efficiency Enabled by in Situ Ionic Liquid Bonding to Cover Carbon Surface Defects. *J. Mater. Chem. A* **2016**, *4* (1), 241−249.

(78) Mirigliano, M.; Borghi, F.; Podestà, A.; Antidormi, A.; Colombo, L.; Milani, P. Non-Ohmic Behavior and Resistive Switching of Au Cluster-Assembled Films beyond the Percolation Threshold. *Nanoscale Advances* **2019**, *1* (8), 3119−3130.

(79) Zhou, G.; Jiang, K.; Wang, Z.; Liu, X. Insight into the Behavior at the Hygroscopicity and Interface of the Hydrophobic Imidazolium-Based Ionic Liquids. *Chin. J. Chem. Eng.* **2020**, DOI: 10.1016/j.cjche.2020.09.047.

SUPPORTING INFORMATION

Nanoconfinement of Ionic Liquid into Porous Carbon Electrodes

Francesca Borghi*,[1], Claudio Piazzoni[1], Matteo Ghidelli[2], Paolo Milani[1], Alessandro Podestà**,[1]

[1] CIMaINa and Dipartimento di Fisica "Aldo Pontremoli", Università degli Studi di Milano, via Celoria 16, 20133 Milano, Italy.

[2] Laboratoire des Sciences des Procédés et des Matériaux (LSPM), CNRS, Université Sorbonne Paris Nord, 93430, Villetaneuse, France.

* Corresponding author: francesca.borghi@unimi.it

** Corresponding author: alessandro.podesta@mi.infn.it

Deposition of evaporated gold and nanostructured carbon for supercapacitor
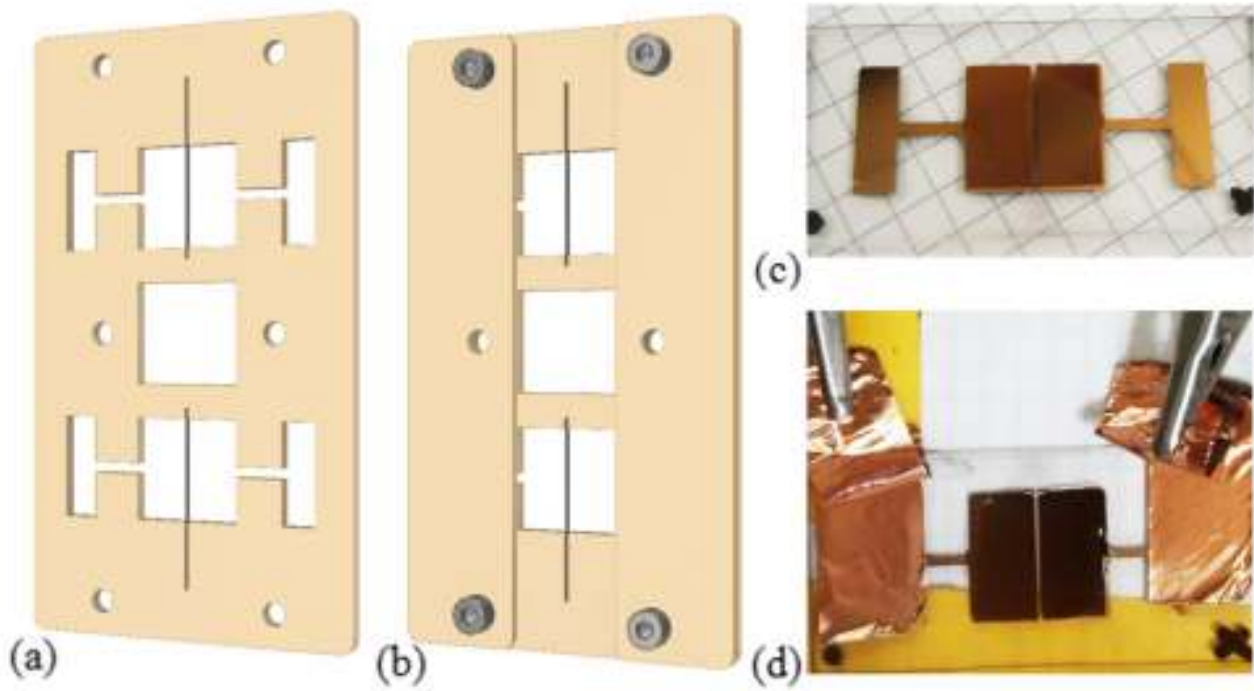

Figure S1. Scheme of the stencil mask used for the evaporation of the gold electrodes (a) and the deposition of the nanostructured carbon thin films (b) by SCBD. The resulting supercapacitor (c) and the configuration of the electrodes during electrochemical measurements (d).
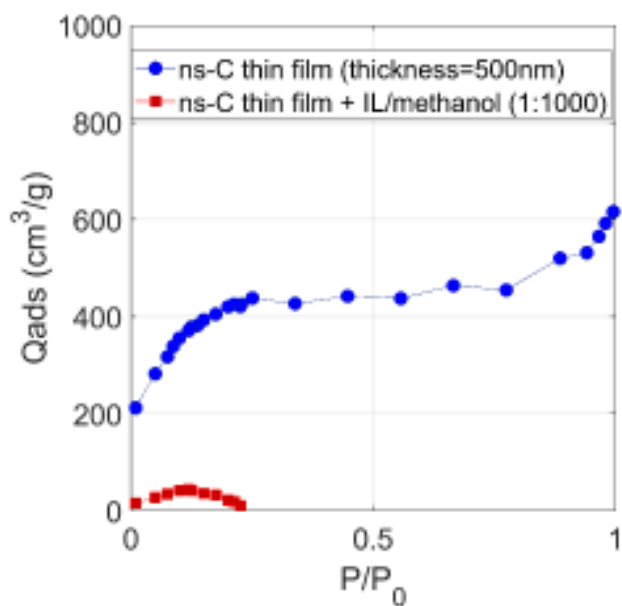
Nitrogen adsorption isotherms

Figure S2. Nitrogen adsorption isotherms of the ns-C sample acquired before and after the ionic liquid deposition onto it.

The adsorption isotherm acquired on the pristine carbon cluster-assembled thin film (the blue dots in Figure S2) is of type I, as commented in Ref.s[1,2], indicating that the sample is microporous. The same carbon sample covered by 300 μl of 1:1000 [Bmim][NTf2]/methanol solution, which does not show ionic liquid traces on the surface accessible by the AFM probe, provides an adsorption isotherm whose shape reveals the drastic decrease of the surface area available by the nitrogen: the adsorbing interface has been reduced so much to be below the minimum measurable by the instrument, and the measurement results to be unreliable.

Evaluation of the coverage of the structured ionic liquid on ns-C thin film

The evaluation of the percentage of coverage of structured IL formed on the ns-C thin film, consists in the acquisition of several images by SEM (as the one reported in Figure S3.a), with a resolution between 1 and 4 nm per pixels, in the binarization of the grayscale images through the choice of a threshold (Figure S3.b), and the evaluation of the area occupied by these objects (the yellow ones in Figure S3.b). The binarization has been carried out by choosing a threshold in a normalized gray-scale with values between 0 and 1 to segment the image distinguishing between the ionic liquid in its liquid phase covering the nanostructured carbon surface (below the threshold, in blue) and the structured IL (above the threshold, in yellow).
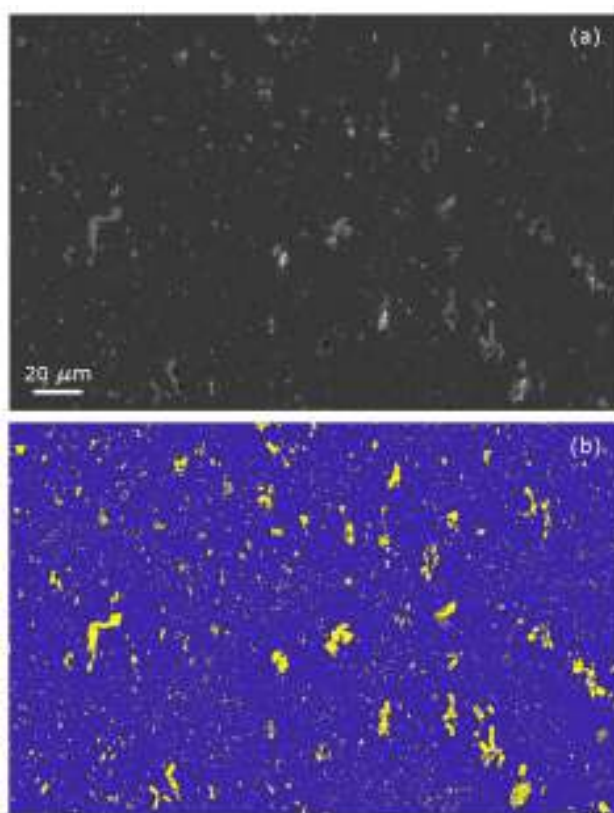

Figure S3. (a) SEM image acquired with low magnification of SMP1 sample covered by [Bmim][NTf2] and (b) the binarized image used for the identification of contrasted structured ionic liquid objects.

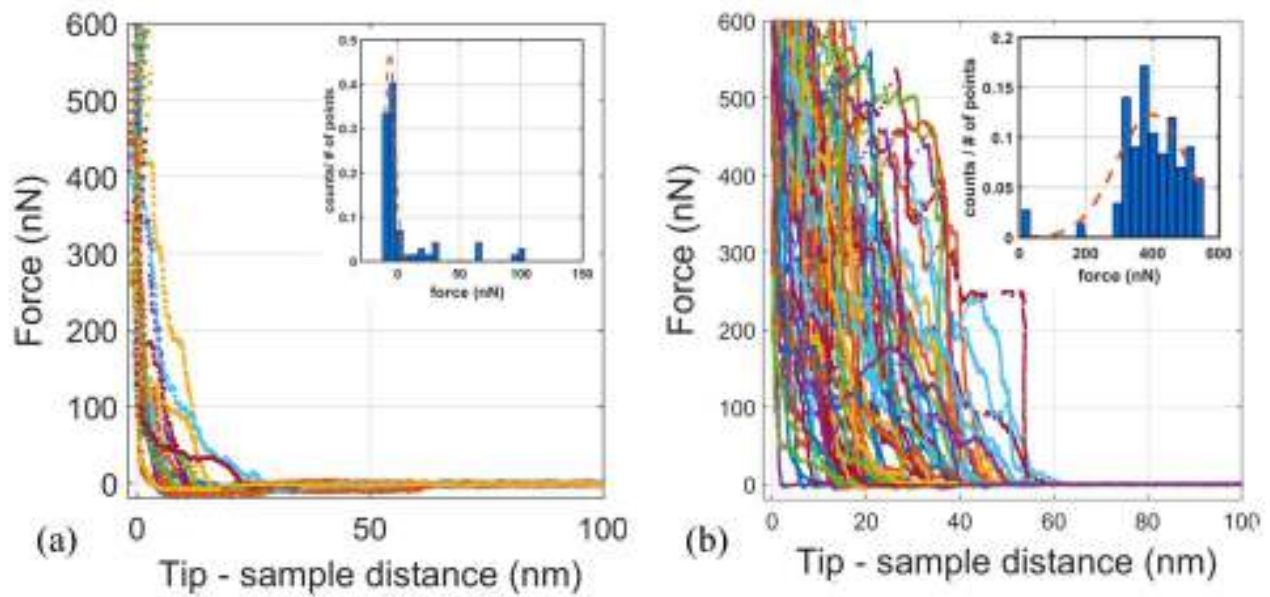# Force spectroscopy on ns-C thin films

Figure S4. Force curves acquired on as-deposited SMP1 ns-C (a) and on as-deposited SMP2 ns-C sample (b). In the insets, the distributions of the forces corresponding to the rupture events are shown.

References

(1) Haul, R. S. J. Gregg, K. S. W. Sing: Adsorption, Surface Area and Porosity. 2. Auflage, Academic Press, London 1982. 303 Seiten, Preis: $ 49.50. *Berichte der Bunsengesellschaft für physikalische Chemie* **1982**, *86* (10), 957–957. https://doi.org/10.1002/bbpc.19820861019.

(2) ALOthman, Z. A Review: Fundamental Aspects of Silicate Mesoporous Materials. *Materials* **2012**, *5* (12), 2874–2902. https://doi.org/10.3390/ma5122874.